Journal of Medicinal Chemistry Article

J. Med. Chem. **2010,** *53,* 5523–5535 **5523**
DOI: 10.1021/jm100183e

Identification of the First Low-Molecular-Weight Inhibitors of Matriptase-2

Mihiret Tekeste Sisay,[‡,§] Torsten Steinmetzer,[†] Marit Stirnberg,[‡] Eva Maurer,[‡] Maya Hammami,[†] Jürgen Bajorath,*[,§] and Michael Gütschow*[,‡]

[‡]*Pharmaceutical Institute, Pharmaceutical Chemistry I, University of Bonn, An der Immenburg 4, D-53121 Bonn, Germany,* [§]*Department of Life Science Informatics, B-IT, Limes Program Unit Chemical Biology and Medicinal Chemistry, University of Bonn, Dahlmannstrasse 2, D-53113 Bonn, Germany, and* [†]*Institute of Pharmaceutical Chemistry, Philipps University Marburg, Marbacher Weg 6, D-35032 Marburg, Germany*

Received February 11, 2010

As recently discovered, matriptase-2, a type II transmembrane serine protease, plays a crucial role in body iron homeostasis by down-regulating hepcidin expression, which results in increased iron levels. Thus, matriptase-2 represents a novel target for the development of enzyme inhibitors potentially useful for the treatment of systemic iron overload (hemochromatosis). A comparative three-dimensional model of the catalytic domain of matriptase-2 was generated and utilized for structure-based virtual screening in combination with similarity searching and knowledge-based compound design. Two N-protected dipeptide amides containing a 4-amidinobenzylamide as P1 residue (compounds **1** and **3**) were identified as the first small molecule inhibitors of matriptase-2 with K_i values of 170 and 460 nM, respectively. An inhibitor of the closely related protease matriptase (compound **2**, K_i = 220 nM), with more than 50-fold selectivity over matriptase-2, was also identified.

Introduction

The vast majority of known serine proteases are either secreted or sequestered in the cytoplasmic storage organelles awaiting signal-regulated release. Over the last years, a structurally distinct new class of serine proteases has been identified that are transmembrane proteins containing an extracellular trypsin-like serine protease domain.[1] These enzymes are ideally positioned to interact with other proteins and mediate the proteolysis of various proteins on the cell surface, of the extracellular matrix, and on adjacent cells. Therefore, localization to the cell surface gives these proteases an excellent opportunity to regulate signal transduction between cells and their extracellular environment. Even though the exact pathophysiological roles of many membrane anchored serine proteases remain to be elucidated, a number of these proteases are indicated to be involved in different stages of cancer progression including growth, invasion, migration, and metastasis,[1−7] and also in several important physiological functions such as digestion, cardiac function and blood pressure regulation, hearing, iron metabolism, and epithelial homeostasis.[2,4,6,8]

The family of type II transmembrane serine proteases (TTSPs[a]) possess a short intracellular N-terminal tail, a transmembrane domain, and a large extracellular portion containing a variable stem region and a C-terminal serine protease catalytic domain of the chymotrypsin fold.[1,2,5,8] The TTSPs can be divided into four subfamilies based on the phylogenetic analysis of the serine protease domain and the stem region. These include the hepsin/TMPRSS subfamily, the human airway trypsin-like protease (HAT) differentially expressed in squamous cell carcinoma (DESC) subfamily, the matriptase subfamily, and corin as the representative of a further subfamily. The members of the matriptase subfamily represent recently identified TTSPs with a unique stem composition and phylogenetically related serine protease domains. Known members of the matriptase subfamily are matriptase,[9,10] matriptase-2,[11] matriptase-3,[12] and the mosaic polyprotease, polyserase-1,[13] as well as its shorter splice-variant termed serase-1B.[14]

Matriptase (membrane-type serine protease 1, MT-SP1, suppressor of tumorigenicity 14), the most studied representative of the matriptase subfamily, was originally identified with a novel gelatinolytic activity in human breast cancer cells.[10] By activating its potential substrates, e.g. pro-single-chain urokinase-type plasminogen activator (pro-uPA) and the proform of hepatocyte growth factor (HGF/scatter factor), matriptase seems to play a relevant role in extracellular matrix degradation and cell scattering, whereas the cleavage of profilaggrin is important for epithelial development.[5,7,15,16] Matriptase was shown to be overexpressed in a vast array of human tumors of epithelial origin including breast, prostate, and ovarian cancers and has been implicated in tumor growth and metastasis in murine models of prostate cancer.[7,9,10,17,18] Therefore, selective inhibition of matriptase has therapeutic potential for the treatment of growth and metastasis of cancer.

On the other hand, matriptase-2 (TMPRSS6, transmembrane serine protease 6), was first identified in 2002 by Velasco and co-workers as a novel membrane-bound mosaic serine protease predominantly expressed in the liver.[11] The extracellular stem region of matriptase-2 consists of a SEA (sea urchin sperm protein, enteropeptidase, agrin) domain-like

*To whom correspondence should be addressed. J.B.: phone, +49 228 2699 306; fax, +49 228 2699 341; E-mail, bajorath@bit.uni-bonn.de. For M.G.: phone, +49 228 732317; fax, +49 228 732567; E-mail, guetschow@uni-bonn.de.

[a]Abbreviations: TTSPs, type II transmembrane serine proteases; PDB, Protein Data Bank; HEK, human embryonic kidney; MOE, Molecular Operating Environment; Tc, Tanimoto coefficient, HepG2, hepatocellular carcinoma, human; FBS, fetal bovine serum.

Published on Web 07/14/2010

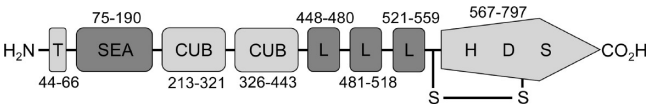

Figure 1. Modular structure of matriptase-2. Different domains are labeled as follows: T, transmembrane domain; SEA, sea urchin sperm protein, enteropeptidase, agrin domain; CUB, complement factor C1s/C1r, urchin embryonic growth factor, bone morphogenetic protein 1 domain; L, low density lipoprotein receptor class A domain. HDS indicates the catalytic triad of the catalytic domain.

region, two CUB (complement factor C1s/C1r, urchin embryonic growth factor, bone morphogenetic protein 1) domains, and three repeats of LDLRA (low density lipoprotein receptor class A) domains (Figure 1).[1,2,11,19,20]

In contrast to matriptase, recent studies have shown that expression of matriptase-2 correlates with suppression of the invasiveness and migration of breast and prostate cancer cells.[21,22] However, precise functions of matriptase-2 in cancer remain to be further elucidated. Another interesting finding that recently attracted much attention is the correlation between mutations in the gene encoding matriptase-2 and iron-refractory iron-deficiency anemia (IRIDA).[23−26] Iron is an essential trace element in mammalian metabolism, and due to its generation of bioreactive superoxide anions and hydroxyl radicals, levels of plasma iron require tight regulation.[26,27] Hepcidin, a small peptide hormone synthesized in the liver, is the homeostatic regulator of plasma iron levels and iron tissue distribution. It inhibits iron absorption from the intestine, regulates iron recycling and release from iron stores, and controls iron transport through the placenta. Hepcidin mediates the internalization and degradation of the iron exporter ferroportin, located on the surface of intestinal enterocytes, macrophages, and hepatocytes, thereby inhibiting iron release into the plasma.[26] As such, control of hepcidin expression represents a critical checkpoint for maintaining iron balance.[28,29] Matriptase-2 suppresses hepcidin expression through proteolytic processing of cell surface hemojuvelin,[23,25,26,30−32] a membrane-bound protein promoting hepcidin expression.[28,33,34] Because of the involvement in such a critical physiological process, matriptase-2 emerges as a potentially important pharmaceutical target. Therefore, selective matriptase-2 inhibitors could be beneficial as pharmacological tools to further investigate its exact role in regulating iron homeostasis and might also be used for therapeutic intervention of frequent iron disorders such as systemic iron overload (hemochromatosis) or iron loading anemias where the level of hepcidin is inappropriately low.

Although peptide-based matriptase-2 inhibitors, i.e., aprotinin and leupeptin, have previously been reported,[11,35] small molecule matriptase-2 inhibitors have not been developed so far. Herein, we report on the generation of a model of the catalytic domain of matriptase-2 and its application in virtual screening and compound evaluation. The model was used to interactively design four substrate-analogue inhibitors, two amidino- and two chloro-substituted benzylamides. A virtual screening campaign was carried out in the presence of these compounds. On the basis of the screening calculations, the designed benzamidines were assigned a high priority. We synthesized these four substrate analogue inhibitors and investigated their inhibitory profile in in vitro assays, leading to the identification of the first low-molecular-weight inhibitors of matriptase-2.

Results and Discussion

Modeling of the Catalytic Domain of Matriptase-2. Because an X-ray crystal structure of human matriptase-2 is currently not available, we attempted to model the structure of the catalytic domain of matriptase-2. The model was generated using crystal structures of closely related enzymes by homology modeling, a procedure by which the coordinates of atoms of a target protein are predicted based on a topological sequence alignment of the target and a template protein(s) of known structure.[36] In a previous study, as part of the first characterization of the enzyme, a 3D model of matriptase-2 was built by means of a semiautomated modeling server.[11] However, because it was intended to utilize the model for inhibitor design, we generated a computer model of matriptase-2 with extensive manual intervention in order to ensure high accuracy of the model in the active site region.

We carried out a sequence search in the Protein Data Bank (PDB)[37] using the amino acid sequence of the catalytic domain of matriptase-2 as query. As expected, the catalytic domain of matriptase showed the highest sequence identity (45%, PDB ID 1EAX), followed by plasma kallikrein (42%, 2ANY), coagulation factor XIa (40%, 1ZSK), the catalytic domain of hepsin (40%, 1Z8G), plasminogen (40%, 1QRZ), α-tryptase (39%, 2F9N), and thrombin (37%, 1ETS). Among available X-ray crystallographic structures of matriptase, the one with highest resolution (1EAX, 1.30 Å)[38] was taken as a primary template. In addition, structure-based multiple sequence alignment was carried out among matriptase-2 and its close homologues (matriptase, plasma kallikrein, hepsin, thrombin) as well as the prototype enzymes factor Xa and trypsin. This procedure provided additional information about conserved and variable regions of matriptase-2 compared to the homologous enzymes. Gaps in the initial alignment were manually adjusted prior to modeling. The optimal sequence alignment of the catalytic domains of matriptase and matriptase-2 (Figure 2A) extracted from the multiple alignment reflects the high degree of similarity between the two enzymes. The major difference occurs in the so-called "60 insertion loop", where matriptase has a nine-residue insertion (DDRGFRYSD), three amino acids longer than that in matriptase-2 (EDSMAS).[38] Two additional single residue deletions in matriptase-2 are located within the "37 loop" and the "70−80 loop" of matriptase.[38]

On the basis of the final sequence alignment, we then generated initial 3D models with three different modeling tools (see Experimental Section). Comparative analysis of these initial models revealed that notable differences between these models were limited to the loop regions and regions of insertions and deletions described above. To model the "60 insertion loop" and regions of insertions and deletions, alternative loops were generated and evaluated. Finally, loop conformations were selected that most closely followed the spatial paths of the corresponding loops in the high-resolution X-ray structure of matriptase. Particular attention was given to the side chain rotamers of nonconserved residues within the active site region. These side chain conformations were adjusted manually by selecting low energy rotamers that matched the side chain pose of the corresponding residues in matriptase as much as possible. After controlled energy refinement (see Experimental Section), the final model of the matriptase-2 catalytic domain displayed good stereochemical quality (with 89% of the residues falling in the most favored regions of the Ramachandran plot) and sequence−structure compatibility

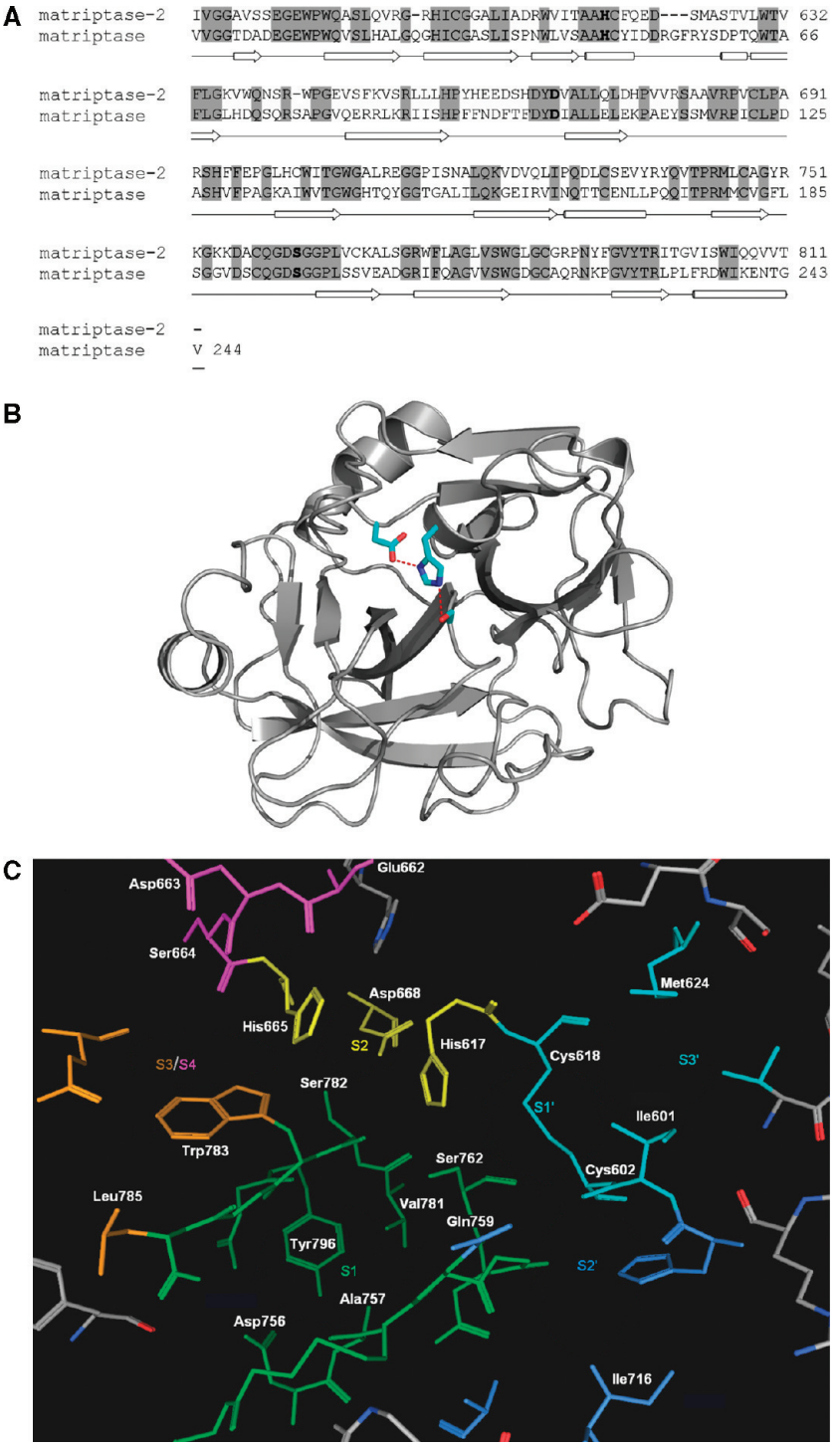

Figure 2. Model generation. (A) Structure-oriented sequence alignment of the catalytic domains of matriptase and matriptase-2 providing the basis for modeling. Amino acid numbers for human matriptase-2 are given for the complete sequence of the enzyme.[20] Numbering for human matriptase is based on chymotrypsinogen numbering.[38] Residues of the catalytic triad are shown in bold, and conserved residues are shaded in gray. Secondary structure elements in the X-ray structure of matriptase are indicated with flat arrows (β-sheets) and cylinders (α-helices).[38] (B) Cartoon representation of the final model of the catalytic domain of matriptase-2 representing the chymotrypsin fold. The catalytic triad is shown in stick presentation. The picture was generated with PyMol.[66] (C) Residues in the active site region of matriptase-2 are shown in stick representation and color-coded according to the pocket they form.

comparable to experimental structures (with a ProSA z-score of 8.13). Stereochemical and sequence-structure compatibility quality control data for the model are provided in the Supporting Information (Figures S1−S3), confirming the overall good quality of the model. However, it is important to note that the major criterion for modeling accuracy in this case has been the close resemblance of the matriptase and matriptase-2 active sites. This has made it possible to apply a rather conservative modeling strategy to generate the matriptase-2 active site model. Because we intended to utilize the model for inhibitor design, this has been the most important aspect of model building and assessment.

Model Analysis. Chymotrypsin-like serine proteases display a common fold (Figure 2B), and their distinct properties arise from sequence differences in the substrate binding region that modulate the shape and chemical nature of binding pockets. The modeled active site structure of matriptase-2 with the amino acid residues forming the corresponding pockets is displayed in Figure 2C. At the center lies the S1 specificity pocket. The backbone of Trp783 (chymotrypsinogen numbering 215), Gly784(216), Gln759(192), and the Cys758(191)−Cys787(220) disulfide bridge form the entrance of the pocket, Gly794(226), Tyr796(228), and Val781(213) form the inner wall, and a critical, specificity determining residue, Asp756(189), is located at the bottom of the S1 pocket. Matriptase-2 has an alanine at the subsequent position 757(190), similar to plasma kallikrein, factor Xa and thrombin, whereas matriptase, trypsin, and uPA have a serine residue at this position. This makes the bottom of the S1 pocket of matriptase-2 slightly more hydrophobic compared to matriptase. Binding of arginine to the S1 site is stabilized by a direct salt bridge between its guanidinium group and the carboxylate group of Asp756(189). However, it is also known that binding of a P1-lysine residue involves the formation of a hydrogen bond to the hydroxyl group of serine and, therefore, less preferred for proteases with alanine at the bottom of the S1 pocket.[39] Accordingly, arginine at the P1 position of peptidic substrates is preferred by matriptase-2.[11,35] The S2 binding site is bordered by His665(99) and His617(57) located above Asp668(102) and Ser782(214). His665(99) separates the small S2 site from the large S3/S4 pocket. This pocket lies to the left of the S1 site, on top of the Trp783(215) indol. The lower part of the S3/S4 extends to Leu785(217), making this spot more hydrophobic compared to matriptase, which has an aspartic acid instead of leucine at the corresponding position. The upper part of the S3/S4 pocket is formed by the backbone carbonyl oxygens of Glu662(96), Asp663(97), and Ser664(98) (corresponding to Asp, Phe, and Thr in matriptase, respectively), representing a negatively charged environment. This part accepts a positively charged residue as has been shown in a substrate mapping study.[35] Different from matriptase, where the benzyl group of Phe97 creates a solvent shield, these residues are solvent exposed. The S1′ pocket is located just above the disulfide bridge Cys602(42)−Cys618(58) between the catalytic His617(57) and the side chain of Ile601(41), whereas the S3′ site is adjacent to the S1′ pocket and bordered by Met624(60D). The S2′ pocket lies in a cleft between Gln759(192) and Ile716(151). This pocket is smaller than that of matriptase due to the substitution of a glycine by isoleucine at position 716.

Inhibitor Design and Virtual Screening Analysis. With the aid of the modeled active site of matriptase-2, shown in Figure 2C, we manually designed four substrate analogue inhibitors. The structures of known potent inhibitors of matriptase,[40] the X-ray structure of a matriptase/inhibitor complex (shown in Figure 3A), and comparison of active site features, as discussed above, were taken into account to support these modeling approach. Specifically, we first focused our design efforts on the deep S1 pocket where the critical negatively charged Asp756(189) residue must interact with an inhibitor in a complementary fashion. Therefore, we first placed a positively charged benzamidine group into this pocket and, as an alternative, a benzene ring with a 2-aminomethyl-5-chloro substitution pattern. This moiety has previously been observed in thrombin inhibitors as a suitable substitute for benzamidine.[41−43] We considered introducing the chlorine at this ring system in order to build in a favorable lipophilic contact with Tyr796(228) inside the S1 pocket.

Having designed the S1 anchor points, we next focused on the small S2 pocket in matriptase-2. A proline could be well placed into this small pocket, which also provided a linker to S3/S4 site. A prominent feature of the upper part of the S3/S4 site in matriptase-2 is the arrangement of backbone carbonyl groups of residues Glu662(96), Asp663(97), and Ser664(98), as discussed above. To complement the negatively charged environment, an arginine residue could be well utilized, reaching into the upper part of the pocket. However, D-configuration of this arginine residue was essential to direct the side chain into the upper part of the S3/S4 pocket. As a control, we also designed test compounds with a D-cyclohexylalanine instead of the D-arginine at this position. This hydrophobic moiety is expected not to reach into the charged upper region of the pocket, but to interact with the lower hydrophobic part of the S3/S4 pocket. A common *N*-terminal benzylsulfonamide group was chosen for our manually designed inhibitors as has been incorporated in series of potent substrate analogue inhibitors of related serine proteases.[43−45]

The design effort resulted in four N-protected dipeptide amides as candidate compounds that are shown in Figure 3B. These four compound suggestions originating from "knowledge-based" design were included into a virtual screen for matriptase-2 inhibitors. A set of 15000 ZINC compounds was preselected on the basis of remote chemical and approximate shape similarity to known matriptase inhibitors (see Experimental Section) and subjected to the docking protocol detailed in the Experimental Section. Importantly, test compounds were flexibly docked, and no assumptions about putative compound binding modes were made to restrict the calculations. Compounds **1** and **3** were among the structures we prioritized based on a detailed analysis of the docking results and their relative ranking position (see Supporting Information). We decided to synthesize and test the four manually designed compounds. Future investigations will be directed toward the evaluation of other highly ranked structures as potential inhibitors of matriptase-2 (see Supporting Information).

Synthesis. The convergent synthesis of compound **1** is shown in Scheme 1. The Boc-protected *O*-acetyl hydroxyamidine **5** was used as a precursor for the benzamidine moiety of **1** (and also **3**). Reductive cleavage followed by deprotection of the Boc group provided 4-amidinobenzylamine dihydrochloride (**6**). N_{ω}-Nitro-D-arginine was N-protected with benzyl sulfonylchloride, and the resulting derivative **7** was coupled with proline methyl ester. Saponification and subsequent catalytic hydrogenation to remove the nitro group afforded the dipeptide **8**. The final compound **1** was then obtained by PyBOP-mediated amide coupling. To prepare the dipeptide amide **2** (Scheme 2), the benzylamine derivative **9**[46] was reacted in a similar manner with **8**. Deprotection of the Boc group was accomplished with TFA to produce **2**. D-Cyclohexylalanine was converted to the sulfonamide **10** (Scheme 3), and the following reaction steps yielded the dipeptide **11** and the final dipeptide amide **3**. The preparation of compound **4** (Scheme 4) was essentially the same as for **2** but started with D-cyclohexylalanine.

Expression of Human Matriptase-2. To study the inhibitory effect of compounds **1**−**4** on human recombinant matriptase-2, the whole matriptase-2 construct was cloned and expressed in human embryonic kidney (HEK) cells with

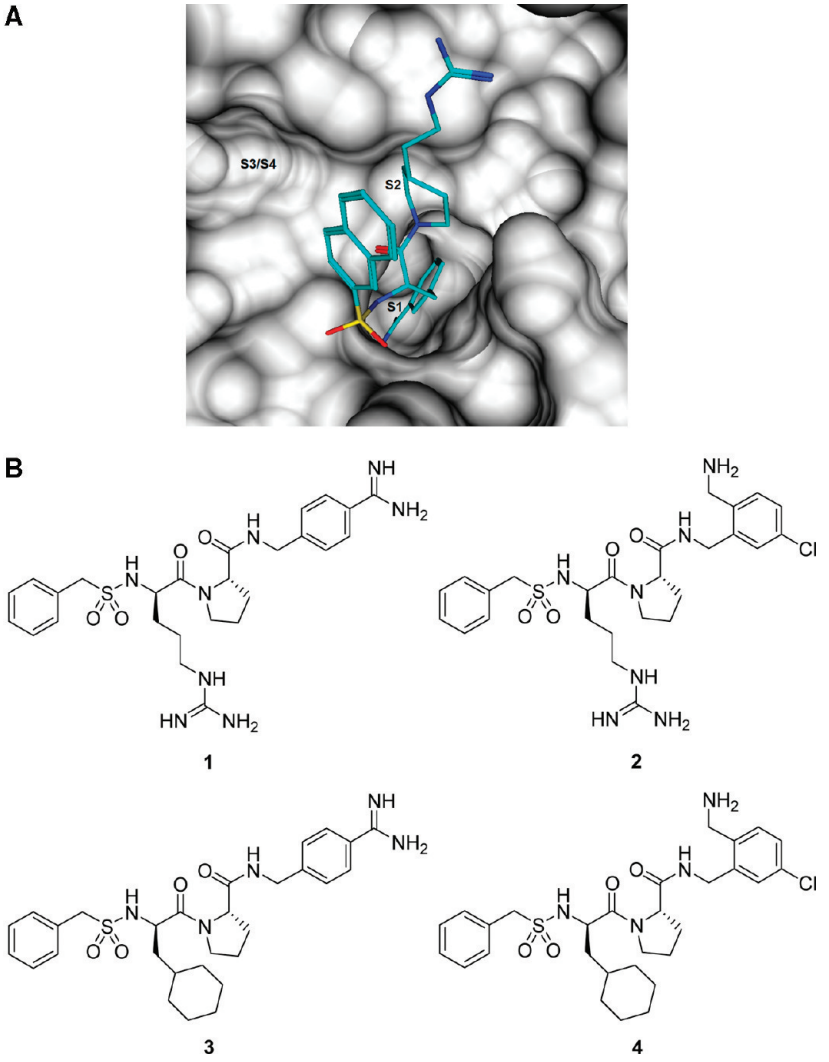

Figure 3. Compound design. (A) shows a crystallographic matriptase inhibitor complex (PDB ID 2GV6) that was used to deduce a likely orientation of putative matriptase-2 inhibitors in the binding site of the homology model. Specificity pockets are labeled. (B) shows the four designed candidate compounds (**1**−**4**).

a Myc-tag at the C-terminal end of the protein. As shown in Figure 4A, an approximately 30 kDa C-terminal fragment of matriptase-2 was detectable using anti-c-Myc antibody in the conditioned medium of transfected HEK cells (HEK-MT2). This form represents the catalytic domain released from the cell surface after processing of the zymogen, as described previously.[32] No signal was detectable in HEK cells expressing the empty vector (HEK-mock). The catalytic domain of matriptase-2 was purified from the conditioned medium of HEK-MT2 cells by immunoaffinity chromatography. After isolation, the purity of matriptase-2 was checked on SDS-Page (Figure 4B). One single band of approximately 30 kDa was visible after purification representing the catalytic domain of matriptase-2.

Enzyme Inhibition Assays. The activity profile of matriptase-2 in the conditioned medium and of the purified catalytic domain of matriptase-2 was characterized using the chromogenic substrate Boc-Gln-Ala-Arg-*para*-nitroanilide. We obtained similar K_m and K_i values (Table 1) from the experiments with either conditioned medium or purified enzyme. Moreover, no detectable activity was observed in the conditioned medium of nontransfected HEK cells or HEK cells expressing the empty vector (HEK-mock). Thus, it is possible to use the conditioned medium as a source for matriptase-2 activity. The K_m values for matriptase-2 in the conditioned medium (210 μM) and for purified matriptase-2 (159 μM) in the micromolar range were similar to human recombinant matriptase (Table 1) and to the reported value (257 μM)[47] for the purified catalytic domain of murine matriptase overexpressed in insect cells measured with the corresponding fluorogenic substrate.

In control experiments, the inhibition of matriptase-2 activity in the conditioned medium and of purified matriptase-2 by aprotinin and leupeptin was measured (Table 1). Similar inhibition of both enzymatic activities was obtained, further confirming that indeed the released matriptase-2 in the conditioned medium accounts for the cleavage of the chromogenic substrate. Aprotinin was more active than leupeptin to inhibit matriptase-2 by at least 2 orders of magnitude, as it has already been found before.[11] Human recombinant matriptase, included in these experiments, was also inhibited by aprotinin in the low nanomolar range. It has been reported that aprotinin, when used at a concentration of 300 nM, led to a nearly complete inhibition of both matriptase and matriptase-2.[35] In accordance to this previous report,[35] a somewhat stronger inhibition of matriptase

Scheme 1[a]

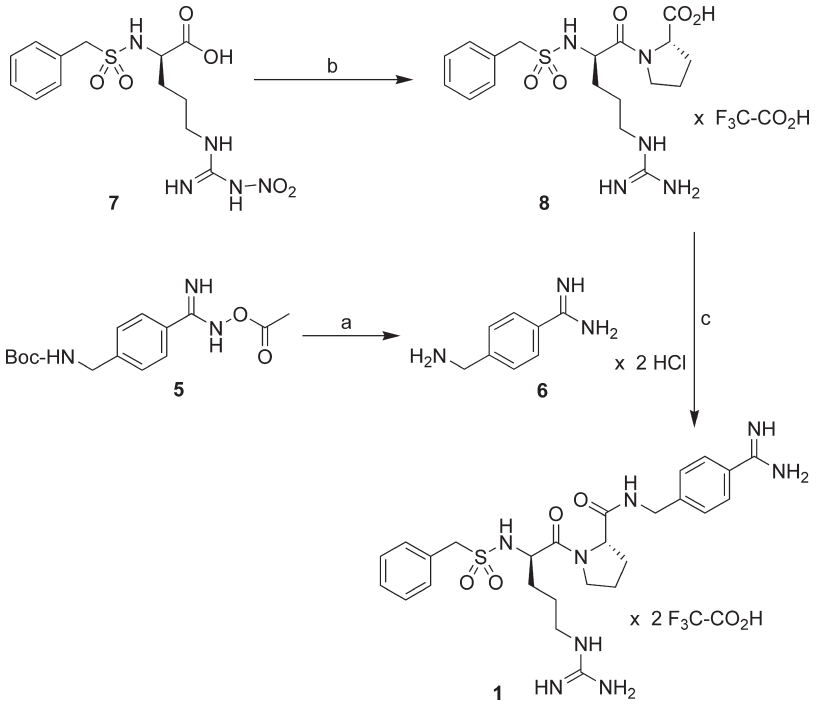

[a] Reagents and conditions: (a) (1) AcOH, H_2, Pd/C; (2) HCl; (b) (1) H-Pro-OMe × HCl, DIPEA, DMF, PyBOP, (2) MeOH, 1 M NaOH (1:1), (3) AcOH, H_2, Pd/C; (c) DIPEA, DMF, PyBOP.

Scheme 2[a]

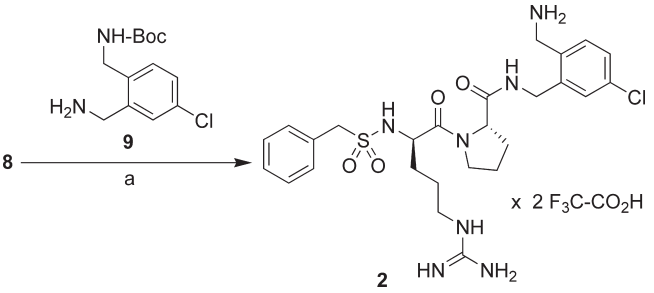

[a] Reagents and conditions: (a) (1) DIPEA, DMF, PyBOP, (2) TFA.

Scheme 3[a]

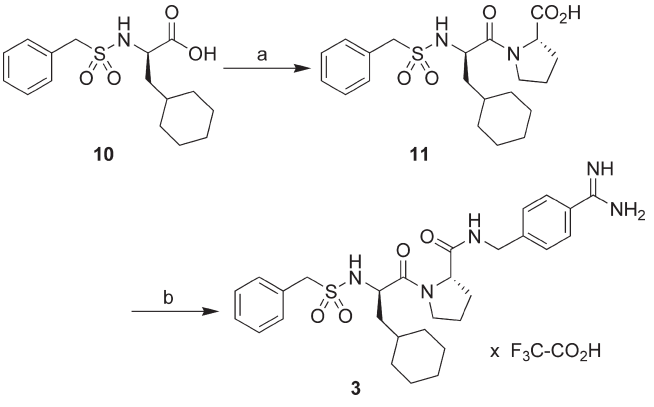

[a] Reagents and conditions: (a) (1) H-Pro-OMe × HCl, DIPEA, DMF, HBTU, (2) MeOH, 1 M NaOH (1:1); (b) compound **6**, DIPEA, DMF, PyBOP.

than matriptase-2 by leupeptin (1.9 μM versus 4.1 μM) was observed.

Scheme 4[a]

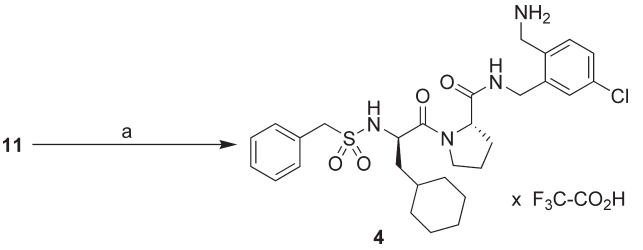

[a] Reagents and conditions: (a) (1) compound **9**, DIPEA, DMF, PyBOP, (2) TFA.

The inhibitory potency of the dipeptide amides **1**−**4** (Figure 3B) toward matriptase-2 was determined and compared with their inhibitory activity against the catalytic domain of the structurally related matriptase (Table 1). Compound **1** containing a D-arginine and a benzamidine moiety was the most potent inhibitor for both enzymes with a 3-fold higher potency for matriptase (K_i = 55 nM) than for matriptase-2 in the conditioned medium (K_i = 190 nM) and purified matriptase-2 (K_i = 170 nM). Dipeptides with a 4-amidinobenzylamide group, such as **1**, are known potent inhibitors of thrombin and factor Xa.[44,48,49] The D-arginine and D-cyclohexylalanine derivatives **2** and **4**, both lacking the benzamidine moiety, had only marginal inhibitory activity against matriptase-2 (K_i > 10 μM). Among the four dipeptide amides, only **3** exhibited a higher potency toward matriptase-2 in the conditioned medium (K_i = 290 nM) and the purified matriptase-2 (K_i = 460 nM) than against matriptase (K_i = 770 nM). As expected for hits arising from a virtual screening approach without selectivity constraints, the inhibitory activity of **1**−**4** is not limited to matriptases. The related serine proteases thrombin and trypsin were also inhibited, and the data are given in the Supporting Information (Table S2).

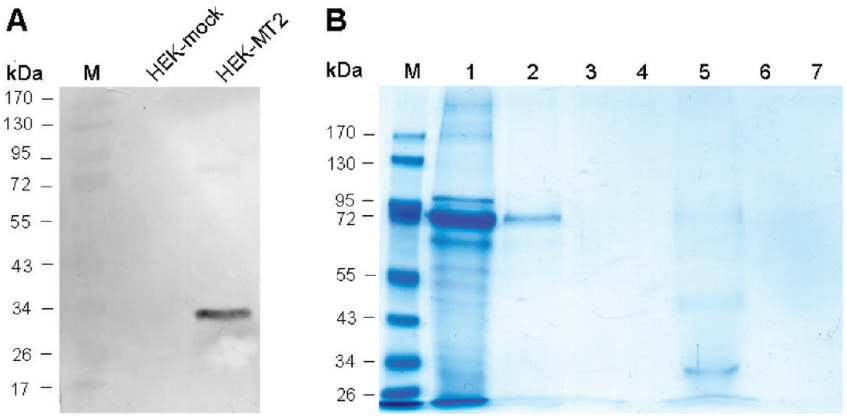

Figure 4. Expression and purification of human matriptase-2. (A) Conditioned medium of HEK cells transfected with an expressing vector harboring matriptase-2 cDNA (HEK-MT2) and without matriptase-2 cDNA (HEK-mock) was characterized by Western blot analysis using anti-c-Myc antibody. (B) The catalytic domain of matriptase-2 was isolated by affinity chromatography using immobilized anti-c-Myc antibody. Lane 1: flow-through; lanes 2−4: wash fractions; lanes 5−7: elution fractions; M: molecular mass markers.

Table 1. Kinetic Parameters for Inhibition of Human Matriptase-2 and Human Matriptase by the Compounds **1**−**4**

	$K_i \pm$ SEM (μM)[a]		
	human matriptase-2		
compd	in conditioned medium of HEK-MT2 cells	purified enzyme	recombinant human matriptase
1	0.19 ± 0.01	0.17 ± 0.02[b]	0.055 ± 0.003
2	> 10[c]	> 10[c]	0.22 ± 0.01
3	0.29 ± 0.02	0.46 ± 0.06	0.77 ± 0.15
4	> 10[c]	> 10[c]	2.1 ± 0.3
aprotinin[d]	0.0050 ± 0.0005	0.013 ± 0.002	0.0098 ± 0.002
leupeptin[d]	2.4 ± 0.2	4.1 ± 0.7	1.9 ± 0.4

[a] IC_{50} values were determined from duplicate measurements with at least five different inhibitor concentrations. K_i values were calculated using the equation $K_i = IC_{50}/(1 + [S]/K_m)$. K_m values obtained for Boc-Gln-Ala-Arg-*para*-nitroanilide were 210 ± 7 μM for matriptase-2 in conditioned medium of HEK-MT2 cells, 159 ± 21 μM for purified matriptase-2, and 381 ± 33 μM for recombinant matriptase. [b] Triplicate measurement with five different inhibitor concentrations. [c] Duplicate measurement with three different inhibitor concentrations. [d] IC_{50} values. Reactions were followed over 20 min to approach steady-state. Steady-state velocities were plotted against inhibitor concentrations to obtain IC_{50} values.

Structure−Activity Relationships. The highly prioritized compounds **1** and **3** were found to be inhibitors of matriptase-2 but not compounds **2** and **4**. Figure 5A shows the final docking pose of the active compound **1**. Because of accuracy limitations, it is generally not possible to predict detailed intermolecular interactions from docked poses, and we do not attempt to do so. However, likely structural characteristics of matriptase-2 inhibition can be explored on the basis of the model. Most probably, the S1 specificity pocket accommodates the benzamidine moiety. Then the amidine group is in contact distance to the side chain of Asp756(189) at the bottom of the S1 pocket. Furthermore, in the docked pose, the guanidino group of arginine occupies the upper part of the S3/S4 pocket and is in contact distance to the carbonyl groups of Glu662(96), Asp663(97), and Ser664(98). In addition, the proline binds to the S2 pocket. The inhibitor forms a short antiparallel β-sheet to the backbone of Ser782-(214) and Gly784(216) as has been experimentally shown in the binding of similar inhibitors to related enzymes.[44,45] The position of the benzylsulfonamide moiety of the inhibitor could not be deduced with a high level of confidence. It resides either at the lower part of the S3/S4 pocket or a shallow hydrophobic subsite behind the S1 binding site, packing against the Cys758(191)−Cys787(220) disulfide bridge. The latter orientation would be supported by the X-ray crystal structure of the complex of factor Xa with a structurally related benzamidine inhibitor where the benzylsulfonamide moiety was located in a corresponding subsite.[44] The binding of compound **3** likely resembles that of compound **1** except that the cyclohexyl group would be positioned within the S3/S4 pocket for favorable interactions with Trp783(215) and Leu785(217) (see Supporting Information, Figure S4).

Compound **1** is also a potent inhibitor of matriptase. When modeled into the binding site of matriptase, it became apparent that the accommodation of the benzylsulfonamide moiety would represent the major difference. In matriptase, this group is oriented toward the lower part of the S3/S4 pocket but could not extend into the shallow hydrophobic subsite behind the S1 pocket because matriptase has a tyrosine residue at position 146 whose side chain would block access of an inhibitor to this subsite (see Supporting Information, Figure S5). The guanidino moiety of **1** extends toward the upper part of the S3/S4 binding pocket forming hydrogen bonding to the Phe97 carbonyl oxygen and cation−π interaction with Phe99 and Trp215, as has been similarly described for other inhibitors of matriptase.[50]

The replacement of D-arginine in **1** by D-cyclohexylalanine in **3** resulted in a stronger decrease in potency against matriptase compared to matriptase-2. This finding might be rationalized by the reduced hydrophobic character of the lower part of the S3/S4 pocket in matriptase compared to matriptase-2. In matriptase-2, the cyclohexyl ring of **3** might favorably interact with Leu-785, but in matriptase, this interaction would be absent and the cyclohexyl ring extends toward the upper part of the S3/S4 pocket (see Supporting

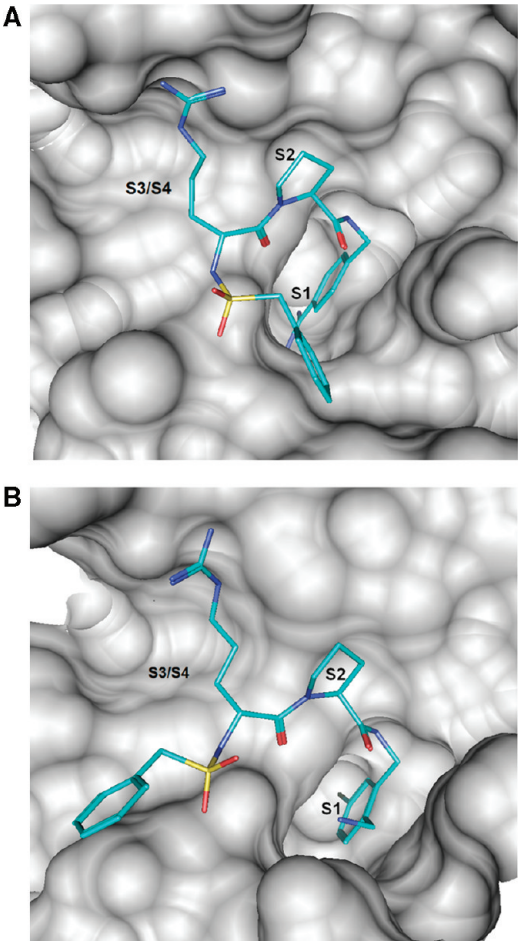

Figure 5. Modeled complexes. (A) Model of the matriptase-2/compound **1** complex. (B) Model of the matriptase/compound **2** complex. Shown are manually adjusted docking poses of these compounds. Specificity pockets are labeled.

Information, Figure S6). In addition, in the case of matriptase, the loss of the cation−π interaction contributes to the decreased activity (**1** versus **3**).

In compounds **2** and **4**, the benzamidine moiety is replaced by a *para*-chlorobenzylamine group. These compounds were inactive against matriptase-2. However, both compounds, in particular **2**, inhibited matriptase. Previously reported X-ray crystal structures of structurally similar inhibitors bound to thrombin[41−43] showed that a chlorobenzene group occupied the S1 pocket with the chloro atom forming a van der Waals contact with Tyr228, which is conserved in matriptase and matriptase-2. Rittle et al. investigated thrombin inhibitors with a chlorobenzene group and introduced an aminomethyl residue in *para*-position to the chlorine, as present in **2** and **4**, which further improved the inhibitory activity. In the X-ray structure, the amino group forms a salt bridge with Glu-192 and a hydrogen bond to Gly-216 at the entrance of the S1 pocket of thrombin.[43] The major difference between matriptase and matriptase-2 inside the S1 pocket is the presence of serine at position 190 in matriptase instead of alanine in matriptase-2. Assuming a binding mode of compounds **2** and **4** in matriptase similar to the one seen in thrombin,[43] which also has alanine at position 190, we would expect the benzamidine−chlorobenzylamine replacement to be tolerated by matriptase-2 rather than matriptase. However, compound **2** was identified as a selective inhibitor of matriptase, which can currently not be rationalized in structural terms. Additional inhibitors with structural variations at the P1 position will be required to better understand selectivity determinants in this case. From the X-ray structure of a related *N*-(3-chlorobenzyl)prolinamide inhibitor in complex with thrombin (PDB ID: 2ZC9),[42] it can be inferred that compound **2** might bind similarly to matriptase as the benzamidine-based inhibitor **1**. However, while the amidine moiety of **1** would interact with Asp189 of matriptase, the chlorobenzylamine group of **2** would be buried inside the S1 pocket and the chloro atom would point toward the aromatic ring of Tyr228. Figure 5B shows a model representing this putative binding mode.

It is also important to note that the docking strategy we applied was not per se validated by reproducing the binding mode of matriptase inhibitors. Rather, the experimental confirmation of inhibitory activity of two of the compounds that we designed and that were highly ranked in our docking calculations supported the approach. On this basis, we also proposed the putative approximate binding mode of these inhibitors, consistent with our design strategy, but also being fully aware of the intrinsic limitations of such predictions, even if they are experimentally supported.

Conclusion

In conclusion, we have identified the first low-molecular-weight inhibitors of matriptase-2. Future investigations will be directed toward structural modifications and the evaluation of their (cyto)toxicity profile. The most potent matriptase-2 inhibitor of this study, compound **1**, was, however, not selective for matriptase-2 over matriptase. Substitution of the guanidine moiety by cyclohexyl slightly reduced the potency against matriptase-2 (**1** versus **3**). This effect, however, is more pronounced in the case of matriptase than matriptase-2, which might be due to the difference in hydrophobic character in the lower part of the S3/S4 pocket and the loss of the cation−π interaction in matriptase. Replacement of the benzamidine by the chlorobenzylamine moiety (**1** and **3** versus **2** and **4**) resulted in a complete loss of inhibitory activity toward matriptase-2. Compound **2** was identified as an inhibitor with strong preference for matriptase over matriptase-2. Such selectivity might be crucial in the development of matriptase inhibitors as anticancer agents because simultaneous inhibition of matriptase-2 is likely to have undesirable effects on body iron metabolism. However, the N-protected dipeptide amides **1** and **3** described herein will be used as leads to develop inhibitors with selectivity toward matriptase-2. The benzamidine substructure present in **1** and **3** is an established pharmacophore in drug development.[45,51,52] Therefore, to improve potency and achieve selectivity toward matriptase-2, future structural modifications might be made while keeping the P1 benzamidine in the molecules. On the other hand, further exploring the P1 site in these compounds is thought to lead to a better understanding of selectivity determinants in matriptases. The selective inhibition of matriptase-2 may serve as a new potential strategy in the treatment of primary hemochromatosis and iron loading anemias.

Experimental Section

General Synthetic Methods and Materials. All reagents including amino acids, amino acid derivatives, coupling reagents, and reagents for synthesis were obtained from Novabiochem, Iris, Fluka, Aldrich, or Acros. 4-Amidinobenzylamine dihydrochloride (**6**) was prepared as described.[53] Analytical HPLC experiments were performed on a Shimadzu LC-10A system

(column: Nucleodur C_{18}, 5 μm, 100 Å, 4.6 mm × 250 mm, Machery-Nagel, Düren, Germany) with a linear gradient of acetonitrile (10−80% in 70 min, detection at 220 nm) containing 0.1% TFA at a flow rate of 1 mL/min. The final inhibitors were purified to more than 95% purity (detection at 220 nm) by preparative HPLC (pumps Varian PrepStar Model 218) using a C_8 column (Nucleodur, 5 μm, 100 Å, 32 mm × 250 mm, Macherey-Nagel, Düren, Germany) and a linear gradient of acetonitrile containing 0.1% TFA at a flow rate of 20 mL/min. All inhibitors were finally obtained as TFA salts after lyophilization. The molecular mass of the synthesized compounds was determined using a QTrap 2000 ESI spectrometer (Applied Biosystems) or an AutoSpek spectrometer (Micromass). The ^{1}H and ^{13}C NMR spectra were recorded on a ECX-400 (Jeol Inc., USA) at 400 and 100 MHz, respectively, and are referenced to internal solvent signals. All tested compounds possessed a purity of at least 95%.

Benzylsulfonyl-N_ω-nitro-D-arginine (7). N_ω-Nitro-D-arginine (4.0 g, 18.25 mmol) was suspended in H_2O (250 mL) and DIPEA (2.36 g, 3.18 mL, 18.25 mmol). The suspension was treated with 3 equiv of benzylsulfonyl chloride (10.44 g, 54.76 mmol) solved in acetonitrile (50 mL) and 6 equiv of DIPEA (14.15 g, 19.05 mL, 109.5 mmol) in several portions at 0 °C over a period of 1 h and was stirred additional 12 h at room temperature. The acetonitrile was removed in vacuo, and the basic aqueous phase was extracted twice with ethyl acetate. The product containing the aqueous phase was acidified by addition of 5% $KHSO_4$ to pH 2−3, partially evaporated, and extracted 3× with ethyl acetate. The organic phase was washed 3× with brine and dried over Na_2SO_4. During evaporation of the solvent, the product starts to crystallize, and compound **7** was obtained (1.9 g, 28%) as white crystals; mp 165−167 °C. MS calcd 373.11, found 374.2 $(M + H)^+$. HPLC: 20.25 min. ^{13}C NMR (DMSO-d_6) δ 24.67 (C_γ-NO_2-Arg), 29.22 (C_β-NO_2-Arg), ca. 40.1 (C_δ-NO_2-Arg), 55.45 (C_α-NO_2-Arg), 58.56 (CH_2SO_2), 127.97, 128.23, 130.23, 130.88 (C_{arom}), 159.30 (C=NH), 173.53 (C=O).

Benzylsulfonyl-D-argininyl-proline Trifluoroacetate (8). Bzls-D-Arg(NO_2)-OH (1.0 g (2.68 mmol), 1.15 equiv of H-Pro-OMe·HCl (0.51 g, 3.08 mmol), and 2.5 equiv of DIPEA (0.87 g, 1.17 mL, 6.7 mmol) were dissolved in DMF (15 mL) at 0 °C and treated with 1.05 equiv of PyBOP (1.46 g, 2.81 mmol). The mixture was stirred at 0 °C for 15 min and then at room temperature overnight. The solvent was removed in vacuo, and the remaining oil was dissolved in ethyl acetate and washed 3× with 5% $KHSO_4$, saturated $NaHCO_3$ solution, and brine, respectively. The organic layer was dried over Na_2SO_4 and evaporated. The remaining residue (1.3 g crude brown oil, HPLC: 29.05 min) was dissolved in methanol (8 mL) and 1 M NaOH (8 mL). The mixture was stirred for 3 h at room temperature and diluted with ethyl acetate and 5% $KHSO_4$. The organic phase was washed 3× with brine, dried over Na_2SO_4, and evaporated. The remaining oil (0.982 g, HPLC 22.67 min, contains approximately 7% of Bzls-D-Arg(NO_2)-OH as impurity) was dissolved in 90% acetic acid (30 mL) and hydrogenated in presence of 10% Pd/C (100 mg) at 35 °C overnight. The catalyst was removed by filtration, the solvent was evaporated in vacuo, and the product was purified by preparative HPLC. The product-containing fractions were combined, evaporated, and lyophilized to obtain compound **8** (0.55 g, 38%) as a white TFA salt; mp < 90 °C (dec). MS calcd 425.17, found 426.2 $(M + H)^+$. HPLC: 18.27 min. ^{13}C NMR (DMSO-d_6) δ 24.75, 25.14 (C_γ-Arg, C_γ-Pro), 29.11, 29.29 (C_β-Arg, C_β-Pro), 40.74 (C_δ-Arg), 47.02 (C_δ-Pro), 54.47 (C_α-Arg), 59.01, 59.20 (C_α-Pro, CH_2SO_2), 128.24, 128.61, 130.64, 131.39 (C_{arom}), 157.23 (C=NH), 170.26, 173.78 (C=O), 116.98 (q, ^1J = 296 Hz, F_3C), 159.11 (q, ^2J = 33 Hz, F_3CCO_2H).

Benzylsulfonyl-D-argininyl-proline-(4-amidinobenzyl)amide Bis(trifluoroacetate) (1). Bzls-D-Arg-Pro-OH·TFA (**8**) (108 mg, 0.20 mmol), 1.1 equiv of 4-amidinobenzylamine·2HCl (**6**)[53] (49 mg, 0.22 mmol), and 2.5 equiv of DIPEA (64 mg, 87 μL, 0.50 mmol) were dissolved in DMF (2 mL) at 0 °C and treated with PyBOP (104 mg, 0.20 mmol). The mixture was stirred at 0 °C for 15 min and 4 h at room temperature. The solvent was removed in vacuo, and the product was purified by preparative HPLC. Product-containing fractions were combined, evaporated, and lyophilized to give compound **1** (95 mg, 60%) as a white powder; mp 161−163 °C. HPLC: 16.8 min. MS calcd 556.25, found 557.2 $(M + H)^+$. ^{13}C NMR (D_2O) δ 24.14, 24.28 (C_γ-Arg, C_γ-Pro), 28.01, 29.39 (C_β-Arg, C_β-Pro), 40.36, 42.80 (C_δ-Arg, NH-CH_2−C_{arom}), 47.73 (C_δ-Pro), 54.95 (C_α-Arg), 59.17, 61.17 (C_α-Pro, CH_2SO_2), 126.21, 127.66, 127.87, 128.43, 128.85, 129.04, 130.83, 144.57 (C_{arom}), 156.78 (NH-C=NH), 165.98 (C_{arom}-C=NH), 172.13, 174.39 (C=O); ca. 116 (F_3C), the TFA CO signal was not detected.

Benzylsulfonyl-D-arginyl-proline-(2-aminomethyl-5-chlorobenzyl)-amide Bis(trifluoroacetate) (2). Bzls-D-Arg-Pro-OH·TFA (**8**) (800 mg, 1.48 mmol), 2-(*tert*-butoxycarbonylaminomethyl)-5-chlorobenzylamine (**9**)[46] (400 mg, 1.48 mmol), and 2 equiv of DIPEA (383 mg, 516 μL, 2.96 mmol) were solved in DMF (15 mL) and treated with PyBOP (770 mg, 1.48 mmol) at 0 °C. The mixture was stirred 15 min at 0 °C and then overnight at room temperature. The solvent was evaporated in vacuo, and the remaining residue (HPLC: 38.81 min) was dissolved in TFA (10 mL). The mixture was stirred at room temperature for 1.5 h, the solvent was removed in vacuo, and the product was purified by preparative HPLC. The product-containing fractions were combined, evaporated, and lyophilized to yield compound **2** (0.64 g, 0.79 mmol) as a white powder; mp 123−125 °C. HPLC: 22.02 min. MS calcd 577.22, found 578.1 $(M + H)^+$. ^{13}C NMR (D_2O) δ 24.17, 24.21 (C_γ-Arg, C_γ-Pro), 28.00, 29.32 (C_β-Arg, C_β-Pro), 39.23, 40.01, 40.40 (C_δ-Arg, NH-CH_2-C_{arom}, NH_2-CH_2), 47.71 (C_δ-Pro), 54.93 (C_α-Arg,), 59.16, 61.01 (C_α-Pro, CH_2SO_2), 128.30, 128.47, 128.74, 128.90, 128.95, 129.10, 130.86, 131.25, 134.94, 138.16 (C_{arom}), 156.75 (C=NH), 172.42, 174.07 (C=O), 116.40 (q, ^1J = 292 Hz, F_3C), 163.00 (q, ^2J = 36 Hz, F_3CCO_2H).

Benzylsulfonyl-D-cyclohexylalanine (10). D-Cyclohexylalanine (2.0 g; 11.68 mmol) was suspended in acetonitrile (90 mL), H_2O (60 mL), and DIPEA (2.03 mL, 1.51 g, 11.68 mmol). The suspension was treated with benzylsulfonyl chloride (6.68 g, 35.05 mmol) and DIPEA (10.17 mL, 7.55 g, 58.4 mmol) in small portions at 0 °C over a period of 1 h and stirred additional 4 h at room temperature. The solvent was removed in vacuo, and the residue was dissolved in a mixture of ethyl acetate and 5% $KHSO_4$. The organic phase was washed 3× with 5% $KHSO_4$ and brine, dried over Na_2SO_4, and evaporated to give **10** (3.1 g, 82%) as a white solid; mp 110−112 °C. MS calcd 325.13, found 348.1 $(M + Na)^+$. HPLC: 45.62 min. ^{13}C NMR ($CDCl_3$) δ 25.85, 26.00, 26.26, 32.26, 33.28, 33.47 ($C_{cyclohexyl}$), 40.84 (C_β-Cha), 54.10 (C_α-Cha), 60.15 (CH_2SO_2), 128.64, 128.79, 128.88, 130.77 (C_{arom}), 177.93 (C=O).

Benzylsulfonyl-D-cyclohexylalanyl-proline (11). Bzls-d-Cha-OH (**10**) (1.34 g, 4.1 mmol), 1.1 equiv of H-Pro-OMe·HCl (0.75 g, 4.5 mmol), and 2.5 equiv of DIPEA (1.324 g, 1.78 mL, 10.25 mmol) were solved in DMF (20 mL) and treated with HBTU (1.55 g, 4.1 mmol) at 0 °C. The mixture was stirred at 0 °C for 30 min and at room temperature overnight. The solvent was removed in vacuo, and the remaining oil was dissolved in ethyl acetate and washed 3× with 5% $KHSO_4$, saturated $NaHCO_3$ solution, and brine, respectively. The organic phase was dried over Na_2SO_4 and evaporated. The remaining ester (2.2 g of amorphous orange solid, HPLC: 53.41 min) was dissolved in methanol (15 mL) and 1 M NaOH (15 mL). The mixture was stirred for 4 h at room temperature and diluted with ethyl acetate and 5% $KHSO_4$. The organic phase was washed 1× with 5% $KHSO_4$ and 3× with brine, dried over Na_2SO_4, and evaporated to give compound **11** (1.3 g, 75%) as a white solid; mp 172−176 °C. MS calcd 422.19, found 423.2 $(M + H)^+$. HPLC: 45.95 min. ^{13}C NMR ($CDCl_3$) δ 24.55, 25.79, 26.06, 26.34, 28.28, 32.13, 33.05, 33.99 ($C_{cyclohexyl}$, C_β-Pro, C_γ-Pro), 41.29 (C_β-Cha), 47.05 (C_δ-Pro), 53.01 (C_α-Cha), 59.68, 59.78 (C_α-Pro, CH_2SO_2), 128.39, 128.69, 129.17, 130.93 (C_{arom}), 172.73, 173.66 (C=O).

Benzylsulfonyl-D-cyclohexylalanyl-proline-(4-amidinobenzyl)-amide Trifluoroacetate (3). First, 250 mg (0.592 mmol) of Bzls-D-Cha-Pro-OH (**11**) (250 mg, 0.59 mmol), 1.1 equiv of 4-amidinobenzylamine·2HCl (**6**)[53] (144 mg, 0.65 mmol), and 3 equiv of DIPEA (309 μL, 229 mg, 1.77 mmol) were solved in DMF (10 mL) and treated with PyBOP (307 mg, 0.59 mmol) at 0 °C. The mixture was stirred 15 min at 0 °C and then 4 h at room temperature. The solvent was evaporated in vacuo, and the product was purified by preparative HPLC. The product-containing fractions were combined, evaporated, and lyophilized to yield compound **3** (0.31 g, 77%) as a white TFA salt; mp 139−141 °C. HPLC: 36.67 min. MS calcd 553.27, found 554.2 $(M + H)^+$. ^{13}C NMR (DMSO-d_6) δ (mixture of conformers, major signals) 23.63, 24.37, 25.55, 25.86, 25.94, 26.04, 29.42, 31.32, 32.99, 33.39 ($C_{cyclohexyl}$, C_β-Pro, C_γ-Pro), 41.67, 44.86, 45.83, 45.87, 46.82 (C_β-Cha, C_δ-Pro, NH-*C*H$_2$-C_{arom}), 52.06 (C_α-Cha), 58.39, 59.95 (C_α-Pro, CH_2SO_2), 126.23, 127.19, 127.67, 127.97, 128.01, 130.40, 130.93, 145.85 (C_{arom}), 165.20 (C=NH), 170.68, 171.94 (C=O), 116.65 (q, ^1J = 297 Hz, F_3C), 158.53 (q, ^2J = 33 Hz, F_3CCO_2H).

Benzylsulfonyl-D-cyclohexylalanyl-proline-(2-aminomethyl-5-chlorobenzyl)amide Trifluoroacetate (4). Bzls-D-Cha-Pro-OH (**11**) (200 mg, 0.473 mmol), 2-(*tert*-butoxycarbonylaminomethyl)-5-chlorobenzylamine (**9**)[46] (128 mg, 0.473 mmol), and 2.5 equiv (206 μL, 153 mg, 1.18 mmol) of DIPEA were solved in DMF (10 mL) and treated with PyBOP (246 mg, 0.473 mmol) at 0 °C. The mixture was stirred 15 min at 0 °C and 4 h at room temperature. The solvent was evaporated in vacuo, and the remaining residue (HPLC: 63.98 min) was dissolved in TFA (10 mL). The mixture was stirred at room temperature for 1.5 h, the solvent was removed in vacuo, and the product was purified by preparative HPLC. The product-containing fractions were combined, evaporated, and lyophilized to give compound **4** (0.24 g, 74%) as a white TFA; mp 118−120 °C. HPLC: 42.17 min. MS calcd 574.24, found 575.1 $(M + H)^+$. ^{13}C NMR (DMSO-d_6) δ (mixture of conformers, major signals) 24.38, 25.53, 25.79, 25.86, 25.94, 26.04, 29.40, 31.27, 32.97, 33.38 ($C_{cyclohexyl}$, C_β-Pro, C_γ-Pro), 38.40, 44.80, 45.83, 45.86, 46.84 (C_β-Cha, C_δ-Pro, NH-*C*H$_2$-C_{arom}, NH_2-CH_2), 52.09 (C_α-Cha), 58.41, 59.94 (C_α-Pro, CH_2SO_2), 126.99, 127.69, 128.01, 128.06, 130.31, 130.46, 130.88, 131.07, 133.29, 139.99 (C_{arom}), 170.67, 172.00 (C=O), 116.93 (q, ^1J = 298 Hz, F_3C), 158.08 (q, ^2J = 33 Hz, F_3CCO_2H).

Template Search, Sequence Alignment, and Model Building. The amino acid sequence of the catalytic domain of matriptase-2 was retrieved from the Swiss-Prot sequence database (http://expasy.org/sprot/), and a template search was performed against sequences of proteins from the PDB[37] using the Basic Local Alignment Search Tool (BLAST) algorithm.[54] Initial pairwise sequence alignments were performed using the ClustalW[55] sequence alignment tool. A structure-based multiple sequence alignment was generated using the protein alignment MOE-Align function of the Molecular Operating Environment (MOE).[56] Three homology modeling software tools, each with different core modeling methods, MOE, Modeller,[36] and the SwissModel modeling server,[57] were used to generate the initial models. All energy minimizations, visualizations, and manual modeling were performed using the MOE graphical environment. To model the "60 insertion loop" and regions of insertions and deletions, alternative loops were generated and evaluated with MOE and the DOPE loop optimization protocol of Modeller. The best intermediate model was selected and subjected to controlled energy minimization while tethering the protein backbone and side chain atoms conserved in matriptase and matriptase-2. The stereochemical quality of intermediate and final refined models was examined using the MOE protein quality evaluation function, an implementation of PROCHECK.[58] Side chain packing quality and sequence−structure compatibility scores were calculated with ProSA-web.[59]

Virtual Screening. The ZINC[60] database containing a total of 5627809 compounds was filtered to remove toxic and reactive compounds and using broadened "rule of five" screen (molecular weight: 200−600; logP: −2−6; donors: 1−10; acceptors: 1−10; rotatable bonds: 0−18), reducing its size to 3684443 unique compounds. Then, eight known inhibitors of matriptase (compounds 2, 8, 18, 20, 29, 31, 56, and 59 from ref 40) were taken as a reference set for nearest neighbor and centroid similarity searching using MACCS structural keys[61] as a fingerprint and the Tanimoto coefficient (T_c)[62] as the similarity measure. Compounds falling into the T_c interval 0.6−0.8 were preselected in order to retain compounds with some structural resemblance to matriptase inhibitors but omit analogues or other notably similar compounds; a total of 206644 compounds from the nearest neighbor search and 203039 from centroid search was obtained. These preselections were reranked using the Molprint2D[63] fingerprint, which is a higher-resolution similarity search tool than MACCS keys, and the top 50000 compounds from each list were taken. Considering compounds occurring in both lists, a total of 67346 unique compounds remained. These database compounds were ranked on the basis of an approximate shape matching procedure using MOE relative to the known matriptase inhibitors, and the top 15000 compounds were then considered for docking and the four manually designed inhibitors were added to this compound pool.

The homology model of matriptase-2 and the matriptase X-ray crystal structure with PDB ID 1EAX[38] were used for docking. As docking programs, DOCK6[64] and FlexX[65] were applied for flexible ligand docking. For FlexX, the active site was prepared by taking all residues into account within 6.5 Å around a crystallographic inhibitor of matriptase (PDB ID 2GV6)[40] after superposition of the homology models and the X-ray structure. For DOCK6, a 10 Å radius was applied to generate and select spheres representing the active site. In both cases, docking parameters were adjusted by redocking the inhibitor of matriptase and reproducing its crystallographic pose.

Initial shape- and energy-based docking calculations were performed with DOCK6, and the final docking and ranking was performed with the FlexX.[65] A total of 2167 compounds produced a DOCK6 energy score of less than −20 kcal/mol. These compounds were redocked using FlexX. Finally, 10 poses of the 30 top-scoring database compounds (see Supporting Information) were visually inspected and 13 compounds were selected as candidates. The selection was mainly based on (i) active site shape/chemical complementarity, (ii) occupation of the S1 specificity pocket by a basic group, (iii) omission of compounds with solvent-exposed hydrophobic groups, and (iv) assessment of conformational strains.

Cell Culture. Human embryonic kidney (HEK) 293 cells, which do not express endogenous matriptase-2 and HepG2 (hepatocellular carcinoma, human) cells expressing matriptase-2, were cultured in Dulbecco's Modified Eagle's medium (DMEM), supplemented with penicillin (100 U/mL), streptomycin (100 μg/mL), glutamine (0.2 M), and fetal bovine serum (10%; FBS; all substances from Invitrogen, Karlsruhe, Germany) under a humidified atmosphere of 5% CO_2.

Cloning and Transfection. Total mRNA was isolated from HepG2 cells expressing endogenous matriptase-2 with TRIZOL-Reagent (Invitrogen, Karlsruhe, Germany) and transcribed into cDNA using Omniscript RT kit (Qiagen, Hilden, Germany) and Oligo dT primer (Invitrogen, Karlsruhe, Germany) according to the instruction manuals. For construction of the expression vector pcDNA4-matriptase-2-Myc-His A, *TMPRSS6* cDNA was obtained by PCR using primers matriptase-2-fw (5′-GCTCCC**GGTACC**ATGCCCGTGGCCGAGGCCC-3′) and matriptase-2-rv (5′-GCTCCC**CTCGAG**GGTCACCACTTGCTGGATCC-3′; *Acc*65I and *Xho*I recognition sites in bold, *TMPRSS6* cDNA underlined). After its cloning into the *Acc*65I/*Xho*I restriction sites of plasmid pcDNA4-Myc-His A (Invitrogen, Karlsruhe, Germany), the

TMPRSS6 DNA fragment was confirmed by sequencing. The resulting expression vector pcDNA4-matriptase-2-Myc-His A encodes the matriptase-2 protein tagged at the C-terminus with a c-Myc epitope (Myc-tag) and six histidine residues (His-tag).

HEK cells were transfected with pcDNA4-matriptase-2-Myc-His A plasmid by lipofection with Lipofectamine TM 2000 (Invitrogen, Karlsruhe, Germany) according to the manufacturer's instructions. Forty-eight hours after transfection, HEK cells were selected with Zeocin (100 μg/mL; Cayla SAS, Toulouse, France). Single cell clones stably expressing the human matriptase-2-Myc-His protein were raised.

Purification and Detection of Matriptase-2. For the purification of the catalytic domain of matriptase-2 from the conditioned medium of transfected HEK-MT2 cells, cells were seeded into 75 cm^2 flasks (5×10^5 cells per cm^2) and cultured for one day in full medium. After two washing steps with PBS media, it was replaced by FBS-free Opti-MEM. Cells were cultured for further two days to increase the protein concentration. Conditioned medium was then collected and concentrated using Amicon Ultra-15 centrifugal filters (3000 MWCO, Millipore, Billerica, MA). To verify expression of matriptase-2, 10 μg of total protein was separated by 10% SDS-PAGE under reducing conditions, analyzed by Western blotting with monoclonal mouse anti-c-myc antibody (clone 9E10; Sigma-Aldrich, Saint Louis, MO) and alkaline phosphatase-conjugated goat anti-mouse IgG (Merck, Darmstadt, Germany). Activity of alkaline phosphatase was visualized with the chromogenic substrate 5-bromo-4-chloro-3-indolyl phosphate (BCIP). The catalytic domain of matriptase-2 was isolated from the concentrated conditioned medium by immunoprecipition using ProFound c-Myc Tag IP/Co-IP Kit (Pierce Biotechnology, Rockford, IL) as described by the manufacturer.

Enzymatic Assay. The activity of matriptase-2 in the conditioned medium of HEK-MT2 cells, of the purified catalytic domain of matriptase-2 and of recombinant matriptase (catalytic domain; Enzo Life Sciences, Lörrach, Germany) was assayed in Tris saline buffer (50 mM Tris, 150 mM NaCl, pH 8.0) at 37 °C by monitoring the release of *para*-nitroaniline from the chromogenic substrate Boc-Gln-Ala-Arg-*para*-nitroanilide (Bachem, Bubendorf, Switzerland) at 405 nm using a Cary 100 UV−vis spectrophotometer (Varian, Darmstadt, Germany). K_m values were determined with eight different substrate concentrations in duplicate experiments. Inhibition assays were performed in duplicate or triplicate measurements with three (**2** and **4** at matriptase-2) or at least five (other experiments) different inhibitor concentrations. IC_{50} values were obtained by nonlinear regression according to equation $v = v_0/(1 + [I]/IC_{50})$. Then 10 mM inhibitor stock solutions of **1**−**4** and leupeptin (Calbiochem. Darmstadt, Germany) and a 100 mM stock solution of Boc-Gln-Ala-Arg-*para*-nitroanilide were prepared in DMSO, and a 1 mM stock solution of aprotinin (Carl Roth, Karlsruhe, Germany) in H_2O. The final concentration of the substrate was 400 μM and of DMSO was 1.5%. Into a cuvette containing 979 μL prewarmed assay buffer, 11 μL of an inhibitor solution and 4 μL of a substrate solution were added and thoroughly mixed. The reaction was initiated by adding 6 μL of an enzyme solution (5 μg/6 μL total protein of the conditioned medium of HEK-MT2 cells; 28 ng/6 μL purified catalytic domain of matriptase-2; 3 ng/6 μL of matriptase) and was followed over 20 min.

Human thrombin (Calbiochem. Darmstadt, Germany) and trypsin from bovine pancreas (Sigma, Steinheim, Germany) were assayed with the chromogenic substrates H-D-Phe-L-Pip-Arg-*para*-nitroanilide (Hyphen BioMed, Neuville-sur-Oise, France) and Suc-Ala-Ala-Pro-Arg-*para*-nitroanilide (Bachem, Bubendorf, Switzerland), respectively. Details are given in the Supporting Information (Table S2).

Acknowledgment. This work was supported by the Graduiertenkolleg 677 and the Sonderforschungsbereich 645 of the Deutsche Forschungsgemeinschaft (DFG). We thank Stephanie Hautmann, Tobias Bald, Stefan Frank, and Maxim Frizler for assistance.

Supporting Information Available: Structures of the 30 top-ranked compounds from the virtual screening experiments. Model evaluation report (Ramachandran diagram, ProSA, and ANOLEA plots). Models of the complex of matriptase-2 with compound **3**, and the complexes of matriptase with compound **1** and **3**, respectively. Data for inhibition of compounds **1**−**4** toward human thrombin and bovine trypsin. ^{13}C NMR spectra of compounds **1**−**4**, **7**, **8**, **10**, and **11**. This material is available free of charge via the Internet at http://pubs.acs.org.

References

(1) Netzel-Arnett, S.; Hooper, J. D.; Szabo, R.; Madison, E. L.; Quigley, J. P.; Bugge, T. H.; Antalis, T. M. Membrane anchored serine proteases: a rapidly expanding group of cell surface proteolytic enzymes with potential roles in cancer. *Cancer Metastasis Rev.* **2003**, *22*, 237–258.

(2) Szabo, R.; Wu, Q.; Dickson, R. B.; Netzel-Arnett, S.; Antalis, T. M.; Bugge, T. H. Type II transmembrane serine proteases. *Thromb. Haemostasis* **2003**, *90*, 185–193.

(3) Noel, A.; Maillard, C.; Rocks, N.; Jost, M.; Chabottaux, V.; Sounni, N. E.; Maquoi, E.; Cataldo, D.; Foidart, J. M. Membrane associated proteases and their inhibitors in tumour angiogenesis. *J. Clin. Pathol.* **2004**, *57*, 577–584.

(4) Bugge, T. H.; Antalis, T. M.; Wu, Q. Type II transmembrane serine proteases. *J. Biol. Chem.* **2009**, *284*, 23177–23181.

(5) Szabo, R.; Bugge, T. H. Type II transmembrane serine proteases in development and disease. *Int. J. Biochem. Cell Biol.* **2008**, *40*, 1297–1316.

(6) Choi, S. Y.; Bertram, S.; Glowacka, I.; Park, Y. W.; Pöhlmann, S. Type II transmembrane serine proteases in cancer and viral infections. *Trends Mol. Med.* **2009**, *15*, 303–312.

(7) Lee, M. S. Matrix-degrading type II transmembrane serine protease matriptase: its role in cancer development and malignancy. *J. Cancer Mol.* **2006**, *2*, 183–190.

(8) Hooper, J. D.; Clements, J. A.; Quigley, J. P.; Antalis, T. M. Type II transmembrane serine proteases. Insights into an emerging class of cell surface proteolytic enzymes. *J. Biol. Chem.* **2001**, *276*, 857–860.

(9) Lin, C. Y.; Anders, J; Johnson, M.; Sang, Q. A.; Dickson, R. B. Molecular cloning of cDNA for matriptase, a matrix-degrading serine protease with trypsin-like activity. *J. Biol. Chem.* **1999**, *274*, 18231–18236.

(10) Shi, Y. E.; Torri, J.; Yieh, L.; Wellstein, A.; Lippman, M. E.; Dickson, R. B. Identification and characterization of a novel matrix-degrading protease from hormone-dependent human breartst cancer cells. *Cancer Res.* **1993**, *53*, 1409–1415.

(11) Velasco, G.; Santiago, C.; Victor, Q.; Luis, M. S.; Carlos, L. Matriptase-2, a membrane-bound mosaic serine proteinase predominantly expressed in human liver and showing degrading activity against extracellular matrix proteins. *J. Biol. Chem.* **2002**, *277*, 37637–37646.

(12) Szabo, R.; Netzel-Arnett, S.; Hobson, J. P.; Antalis, T. M.; Bugge, T. H. Matriptase-3 is a novel phylogenetically preserved membrane-anchored serine protease with broad serpin reactivity. *Biochem. J.* **2005**, *390*, 231–242.

(13) Cal, S.; Quesada, V.; Garabaya, C.; Lopez-Otin, C. Polyserase-I, a human polyprotease with the ability to generate independent serine protease domains from a single translation product. *Proc. Natl. Acad. Sci. U.S.A.* **2003**, *100*, 9185–9190.

(14) Okumura, Y.; Hayama, M.; Takahashi, E.; Fujiuchi, M.; Shimabukuro, A.; Yano, M.; Kido, H. Serase-1B, a new splice variant of polyserase-1/TMPRSS9, activates urokinase-type plasminogen activator and the proteolytic activation is negatively regulated by glycosaminoglycans. *Biochem. J.* **2006**, *400*, 551–561.

(15) Lee, S. L.; Dickson, R. B.; Lin, C. Y. Activation of hepatocyte growth factor and urokinase plasminogen activator by matriptase, an epithelial membrane serine protease. *J. Biol. Chem.* **2000**, *275*, 36720–36725.

(16) List, K.; Szabo, R.; Wertz, P. W.; Segre, J.; Haudenschild, C. C.; Kim, S. Y.; Bugge, T. H. Loss of proteolytically processed filaggrin caused by epidermal deletion of Matriptase/MT-SP1. *J. Cell Biol.* **2003**, *163*, 901–910.

(17) Oberst, M. D.; Johnson, M. D.; Dickson, R. B.; Lin, C. Y.; Singh, B.; Stewart, M.; Williams, A.; Nafussi, A.; Smyth, J. F.; Gabra, H.; Sellar, G. C. Expression of the serine protease matriptase and its

inhibitor HAI-1 in epithelial ovarian cancer: correlation with clinical outcome and tumor clinicopathological parameters. *Clin. Cancer Res.* **2002**, *8*, 1101–1107.
(18) Uhland, K. Matriptase and its putative role in cancer. *Cell. Mol. Life Sci.* **2006**, *63*, 2968–2978.
(19) Park, T. J.; Lee, Y. J.; Kim, H. J.; Park, H. G.; Park, W. J. Cloning and characterization of TMPRSS6, a novel type 2 transmembrane serine protease. *Mol. Cells* **2005**, *19*, 223–227.
(20) Ramsay, A. J.; Reid, J. C.; Velasco, G.; Quigley, J. P.; Hooper, J. D. The type II transmembrane serine protease matriptase-2—identification, structural features, enzymology, expression pattern and potential roles. *Front. Biosci.* **2008**, *13*, 569–579.
(21) Parr, C.; Sanders, A. J.; Davies, G.; Martin, T.; Lane, J.; Mason, M. D.; Mansel, R. E.; Jiang, W. G. Matriptase-2 inhibits breast growth and invasion and correlates with favorable prognosis for breast cancer patients. *Clin. Cancer. Res.* **2007**, *13*, 3568–3576.
(22) Sanders, A. J.; Parr, C.; Martin, T. A.; Lane, J.; Mason, M. D.; Jiang, W. G. Genetic upregulation of matriptase-2 reduces the aggressiveness of prostate cancer cells in vitro and in vivo and affects FAK and paxillin localisation. *J. Cell. Physiol.* **2008**, *216*, 780–789.
(23) Du, X.; She, E.; Gelbart, T.; Truksa, J.; Lee, P.; Xia, Y.; Khovananth, K.; Mudd, S.; Mann, N.; Moresco, E. M. Y.; Beutler, E.; Beutler, B. The serine protease TMPRSS6 is required to sense iron deficiency. *Science* **2008**, *320*, 1088–1092.
(24) Finberg, K. E.; Heeney, M. M.; Campagna, D. R.; Ayşinok, Y.; Pearson, H. A.; Hartman, K. R.; Mayo, M. M.; Samuel, S. M.; Strouse, J. J.; Markianos, K.; Andrews, N. C.; Fleming, M. D. Mutations in TMPRSS6 cause iron-refractory iron deficiency anaemia (IRIDA). *Nat. Genet.* **2008**, *40*, 569–571.
(25) Melis, M. A.; Cau, M.; Congiu, R.; Sole, G.; Barella, S.; Cao, A.; Westerman, M.; Cazzola, M.; Galanello, R. A mutation in the TMPRSS6 gene, encoding a transmembrane serine protease that suppresses hepcidin production, in familial iron deficiency anemia refractory to oral iron. *Haematologica* **2008**, *93*, 1473–1479.
(26) Ramsay, A. J.; Hooper, J. D.; Folgueras, A. R.; Velasco, G.; Lopez-Otin, C. Matriptase-2 (TMPRSS6): a proteolytic regulator of iron homeostasis. *Haematologica* **2009**, *94*, 840–849.
(27) De Domenico, I.; McVey Ward, D.; Kaplan, J. Regulation of iron acquisition and storage: consequences for iron-linked disorders. *Nat. Rev. Mol. Cell. Biol.* **2008**, *9*, 72–81.
(28) Niederkofler, V.; Salie, R.; Arber, S. Hemojuvelin is essential for dietary iron sensing, and its mutation leads to severe iron overload. *J. Clin. Invest.* **2005**, *115*, 2180–2186.
(29) Nemeth, E.; Tuttle, M. S.; Powelson, J.; Vaughn, M. B.; Donovan, A.; Ward, D. M.; Ganz, T.; Kaplan, J. Hepcidin regulates cellular iron efflux by binding to ferroportin and inducing its internalization. *Science* **2004**, *306*, 2090–2093.
(30) Guillem, F.; Lawson, S.; Kannengiesser, C.; Westerman, M.; Beaumont, C.; Grandchamp, B. Two nonsense mutations in the TMPRSS6 gene in a patient with microcytic anemia and iron deficiency. *Blood* **2008**, *112*, 2089–2091.
(31) Folgueras, A. R.; de Lara, F. M.; Pendás, A. M.; Garabaya, C.; Rodriguez, F.; Astudillo, A.; Bernal, T.; Cabanillas, R.; López-Otín, C.; Velasco, G. Membrane-bound serine protease matriptase-2 (Tmprss6) is an essential regulator of iron homeostasis. *Blood* **2008**, *112*, 2539–2545.
(32) Silvestri, L.; Pagani, A.; Nai, A.; De Domenico, I.; Kaplan, J.; Camaschella, C. The serine protease matriptase-2 (TMPRSS6) inhibits hepcidin activation by cleaving membrane hemojuvelin. *Cell Metab.* **2008**, *8*, 502–511.
(33) Papanikolaou, G.; Samuels, M. E.; Ludwig, E. H.; MacDonald, M. L.; Franchini, P. L.; Dubé, M. P.; Andres, L.; MacFarlane, J.; Sakellaropoulos, N.; Politou, M.; Nemeth, E.; Thompson, J.; Risler, J. K.; Zaborowska, C.; Babakaiff, R.; Radomski, C. C.; Pape, T. D.; Davidas, O.; Christakis, J.; Brissot, P.; Lockitch, G.; Ganz, T.; Hayden, M. R.; Goldberg, Y. P. Mutations in HFE2 cause iron overload in chromosome 1q-linked juvenile hemochromatosis. *Nat. Genet.* **2004**, *36*, 77–82.
(34) Malyszko, J. Hemojuvelin: the hepcidin story continues. *Kidney Blood Press Res.* **2009**, *32*, 71–76.
(35) Béliveau, F.; Désilets, A.; Leduc, R. Probing the substrate specificities of matriptase, matriptase-2, hepsin and DESC1 with internally quenched fluorescent peptides. *FEBS J.* **2009**, *276*, 2213–2226.
(36) Sali, A.; Blundell, T. L. Comparative protein modeling by satisfaction of spatial restraints. *J. Mol. Biol.* **1993**, *234*, 779–815.
(37) Berman, H. M.; Westbrook, J.; Feng, Z.; Gilliland, G.; Bhat, T. N.; Weissig, H.; Shindyalov, I. N.; Bourne, P. E. The Protein Data Bank. *Nucleic Acids Res.* **2000**, *28*, 235–242.
(38) Friedrich, R.; Fuentes-Prior, P.; Ong, E.; Coombs, G.; Hunter, M.; Oehler, R.; Pierson, D.; Gonzalez, R.; Huber, R.; Bode, W.; Madison, E. L. Catalytic domain structures of MT-SP1/matriptase, a matrix-degrading transmembrane serine proteinase. *J. Biol. Chem.* **2002**, *277*, 2160–2168.
(39) Sichler, K.; Hopfner, K. -P.; Kopetzki, E.; Huber, R.; Bode, W.; Brandstetter, H. The influence of residue 190 in the S1 site of trypsin-like serine proteases on substrate selectivity is universally conserved. *FEBS Lett.* **2002**, *530*, 220–224.
(40) Steinmetzer, T.; Schweinitz, A.; Stürzebecher, A.; Donnecke, D.; Uhland, K.; Schuster, O.; Steinmetzer, P.; Müller, F.; Friedrich, R.; Than, M. E.; Bode, W.; Stürzebecher, J. Secondary amides of sulfonylated 3-amidinophenylalanine. New potent and selective inhibitors of matriptase. *J. Med. Chem.* **2006**, *49*, 4116–4126.
(41) Stauffer, K. J.; Williams, P. D.; Selnick, H. G.; Nantermet, P. G.; Newton, C. L.; Homnick, C. F.; Zrada, M. M.; Lewis, S. D.; Lucas, B. J.; Krueger, J. A.; Pietrak, B. L.; Lyle, E. A.; Singh, R.; Miller-Stein, C.; White, R. B.; Wong, B.; Wallace, A. A.; Sitko, G. R.; Cook, J. J.; Holahan, M. A.; Stranieri-Michener, M.; Leonard, Y. M.; Lynch, J. J., Jr.; McMasters, D. R.; Yan, Y. 9-Hydroxyazafluorenes and their use in thrombin inhibitors. *J. Med. Chem.* **2005**, *48*, 2282–2293.
(42) Baum, B.; Mohamed, M.; Zayed, M.; Gerlach, C.; Heine, A.; Hangauer, D.; Klebe, G. More than a simple lipophilic contact: a detailed thermodynamic analysis of nonbasic residues in the S1 pocket of thrombin. *J. Mol. Biol.* **2009**, *390*, 56–69.
(43) Rittle, K. E.; Barrow, J. C.; Cutrona, K. J.; Glass, K. L.; Krueger, J. A.; Kuo, L. C.; Lewis, S. D.; Lucas, B. J.; McMasters, D. R.; Morrissette, M. M.; Nantermet, P. G.; Newton, C. L.; Sanders, W. M.; Yan, Y.; Vacca, J. P.; Selnick, H. G. Unexpected enhancement of thrombin inhibitor potency with *o*-aminoalkylbenzylamides in the P1 position. *Bioorg. Med. Chem. Lett.* **2003**, *20*, 3477–3482.
(44) Schweinitz, A.; Stürzebecher, A.; Stürzebecher, U.; Schuster, O.; Stürzebecher, J.; Steinmetzer, T. New substrate analogue inhibitors of factor Xa containing 4-amidinobenzylamide as P1 residue: Part 1. *Med. Chem.* **2006**, *2*, 349–361.
(45) Schweinitz, A.; Steinmetzer, T.; Banke, I. J.; Arlt, M. J. E.; Stürzebecher, A.; Schuster, O.; Geissler, A.; Giersiefen, H.; Zeslawska, E.; Jacob, U.; Krüger, A.; Stürzebecher, J. Design of novel and selective inhibitors of urokinase-type plasminogen activator with improved pharmacokinetic properties for use as antimetastatic agents. *J. Biol. Chem.* **2004**, *279*, 33613–33622.
(46) Nelson, T. D.; LeBlond, C. R.; Frantz, D. E.; Matty, L.; Mitten, J. V.; Weaver, D. G.; Moore, J. C.; Kim, J. M.; Boyd, R.; Kim, P. -Y.; Gbewonyo, K.; Brower, M.; Sturr, M.; McLaughlin, K.; McMasters, D. R.; Kress, M. H.; McNamara, J. M.; Dolling, U. H. Stereoselective synthesis of a potent thrombin inhibitor by a novel P2-P3 lactone ring opening. *J. Org. Chem.* **2004**, *69*, 3620–3627.
(47) Cho, E. G.; Kim, C.; Kim, M. G.; Kim, S. R.; Seong, I. S.; Chung, C.; Schwartz, R. H.; Park, D. N-Terminal processing is essential for release of epithin, a mouse type II transmembrane serine protease. *J. Biol. Chem.* **2001**, *276*, 44581–44589.
(48) Hellstern, P.; Stürzebecher, U.; Wuchold, B.; Haubelt, H.; Seyfert, U. T.; Bauer, M.; Vogt, A.; Stürzebecher, J. Preservation of in vitro function of platelets stored in the presence of a synthetic dual inhibitor of factor Xa and thrombin. *J. Thromb. Haemostasis* **2007**, *5*, 2119–2126.
(49) Stürzebecher, A.; Dönnecke, D.; Schweinitz, A.; Schuster, O.; Steinmetzer, P.; Stürzebecher, U.; Kotthaus, J.; Clement, B.; Stürzebecher, J.; Steinmetzer, T. Highly potent and selective substrate analogue factor Xa inhibitors containing D-homophenylalanine analogues as P3 residue: part 2. *ChemMedChem* **2007**, *2*, 1043–1053.
(50) Steinmetzer, T.; Dönnecke, D.; Korsonewski, M.; Neuwirth, C.; Steinmetzer, P.; Schulze, A.; Saupe, S. M.; Schweinitz, A. Modification of the N-terminal sulfonyl residue in 3-amidinophenylalanine-based matriptase inhibitors. *Bioorg. Med. Chem. Lett.* **2009**, *19*, 67–73.
(51) Steinmetzer, T.; Stürzebecher, J. Progress in the development of synthetic thrombin inhibitors as new orally active anticoagulants. *Curr. Med. Chem.* **2004**, *11*, 2297–2321.
(52) Soeiro, M. N.; de Castro, S. L.; de Souza, E. M.; Batista, D. G.; Silva, C. F.; Boykin, D. W. Diamidine activity against trypanosomes: the state of the art. *Curr. Mol. Pharmacol.* **2008**, *1*, 151–161.
(53) Becker, G. L.; Sielaff, F.; Than, M. E.; Lindberg, I.; Routhier, S.; Day, R.; Lu, Y.; Garten, W.; Steinmetzer, T. Potent inhibitors of furin and furin-like proprotein convertases containing decarboxylated P1 arginine mimetics. *J. Med. Chem.* **2010**, *53*, 1067–1075.
(54) Altschul, S. F.; Madden, T. L.; Schäffer, A. A.; Zhang, J.; Zhang, Z.; Miller, W.; Lipman, D. J. Gapped BLAST and PSI-BLAST: a new generation of protein database search programs. *Nucleic Acids Res.* **1997**, *25*, 3389–3402.
(55) Thompson, J. D.; Higgins, D. G.; Gibson, T. J. ClustalW: improving the sensitivity of progressive multiple sequence alignments

through sequence weighting, position specific gap penalties and weight matrix choice. *Nucleic Acids Res.* **1994**, *22*, 4673–4680.
(56) *Molecular Operating Environment* (*MOE 2005.06*); C.C.G. Inc.: Montreal, Canada, 2005.
(57) Schwede, T.; Kopp, J.; Guex, N.; Peitsch, M. C. SWISS-MODEL: an automated protein homology-modeling server. *Nucleic Acids Res.* **2003**, *31*, 3381–3385.
(58) Laskowski, R. A.; MacArthur, M. W.; Moss, D. S.; Thornton, J. M. PROCHECK: a program to check the stereochemical quality of protein structures. *J. Appl. Crystallogr.* **1993**, *26*, 283–291.
(59) Wiederstein, M.; Sippl, M. J. ProSA-web: interactive web service for the recognition of errors in three-dimensional structures of proteins. *Nucleic Acids Res.* **2007**, *35*, W407–W410.
(60) Irwin, J. J.; Shoichet, B. K. ZINC—a free database of commercially available compounds for virtual screening. *J. Chem. Model.* **2005**, *45*, 177–182.
(61) Durant, J. L.; Leland, B. A.; Henry, D. R.; Nourse, J. G. Reoptimization of MDL keys for use in drug discovery. *J. Chem. Inf. Comput. Sci.* **2002**, *42*, 1273–1280.
(62) Willett, P. Searching techniques for databases of two- and three-dimensional chemical structures. *J. Med. Chem.* **2005**, *48*, 4183–4199.
(63) Bender, A.; Mussa, H. Y.; Glen, R. C.; Reiling, S. Molecular similarity searching using atom environments, information-based feature selection, and a naïve Bayesian classifier. *J. Chem. Inf. Comput. Sci.* **2004**, *44*, 170–178.
(64) Meng, E. C.; Shoichet, B. K.; Kuntz, I. D. Automated docking with grid-based energy evaluation. *J. Comput. Chem.* **1992**, *13*, 505–524.
(65) Rarey, M.; Kramer, B.; Lengauer, T.; Klebe, G. A fast flexible docking method using an incremental construction algorithm. *J. Mol. Biol.* **1996**, *261*, 470–489.
(66) DeLano, W. L. The PyMOL molecular graphics system; DeLano Scientific: San Carlos, CA, 2002; http://www.pymol.org.